11-2011

NEMO5: A Parallel Multiscale Nanoelectronics Modeling Tool

Sebastian Steiger
Purdue University, steiger@purdue.edu

Michael Povolotskyi
Purdue University, mpovolot@purdue.edu

Hong-Hyun Park
Purdue University, park310@purdue.edu

Tillmann Kubis
Purdue University, tkubis@purdue.edu

Gerhard Klimeck
Purdue University, gekco@purdue.edu

Steiger, Sebastian; Povolotskyi, Michael; Park, Hong-Hyun; Kubis, Tillmann; and Klimeck, Gerhard, "NEMO5: A Parallel Multiscale Nanoelectronics Modeling Tool" (2011). *Birck and NCN Publications.* Paper 835.
http://dx.doi.org/10.1109/TNANO.2011.2166164

NEMO5: A Parallel Multiscale Nanoelectronics Modeling Tool

Sebastian Steiger, Michael Povolotskyi, Hong-Hyun Park, Tillmann Kubis, and Gerhard Klimeck, *Senior Member, IEEE*

***Abstract*—The development of a new nanoelectronics modeling tool, NEMO5, is reported. The tool computes strain, phonon spectra, electronic band structure, charge density, charge current, and other properties of nanoelectronic devices. The modular layout enables a mix and match of physical models with different length scales and varying numerical complexity. NEMO5 features multilevel parallelization and is based on open-source packages. Its versatility is demonstrated with selected application examples: a multimillion-atom strain calculation, bulk electron and phonon band structures, a 1-D Schrödinger–Poisson simulation, a multiphysics simulation of a resonant tunneling diode, and quantum transport through a nanowire transistor.**

***Index Terms*—Modeling, multiphysics, multiscale, nanoelectronics, nanostructures, nonequilibrium Greens function formalism (NEGF), NEMO, phonons, Poisson, quantum dot, quantum well, quantum wire, Schrödinger, simulation, strain, transport.**

I. Introduction

DURING the past two decades, the central parts of semiconductor devices shrank to a few or tens of nanometers and a transition took place in the governing physics. Today's transistors are believed to operate in a near-ballistic regime, where a typical carrier experiences few scattering events during its journey across the device. The device operation is largely dictated by the laws of quantum mechanics, the detailed atomistic composition of the devices, and nonequilibrium carrier distributions. To control and optimize such nanoscale devices, physics-based modeling is critical.

In the mid 1990s, NEMO-1D [1] became the first industrial-strength tool to simulate quantum transport in an atomistic basis and coherence loss in layered devices using the nonequilibrium Green's function formalism (NEGF). It enabled the quantitative analysis and prediction of the characteristics of n-type resonant tunneling diodes (RTDs). An accurate electronic band structure beyond effective mass, robust numerics and user-friendliness were key to the success and use of the tool.

The semiempirical tight-binding model in NEMO-1D, based on an atomistic representation of nanostructures, proved to yield highly accurate results. However, the computational cost of bigger structures as well as the lack of a sound model for the influence of strain on the tight-binding Hamiltonian were unresolved issues at the time. NEMO-3D [2] introduced real-space parallelization techniques and strain models to compute quantum states in strained 3-D systems containing millions of atoms [3]. Its improvements allowed for a detailed analysis of quantum-dot emission spectra [4] and silicon impurity properties [5] amongst others. Recently, the spatial decomposition has been generalized to a 3-D scheme, termed NEMO-3D-Peta [6], to calculate properties of even larger Si:P systems for applications in quantum computing.

The synthesis of spatial-domain decomposition and quantum transport was achieved by the code OMEN [7]. With the ability to employ effectively the largest computing resources available [8], OMEN serves today as an active research tool to study post-CMOS devices such as band-to-band tunneling devices [9], high electron mobility transistors (HEMTs) [10] and nanowires [11].

The present tool, NEMO5, has been designed and developed based on these prior experiences and key insights.

1) Atomistic effects like interface roughness, alloy disorder, and impurities are critical to the quantitative understanding of nanoelectronics devices. Thus, an atomistic structure representation is preferred for most investigations of nanoelectronic devices.
2) Cluster computing is becoming ever more important as processors become not faster but cheaper. Excellent scalability and multilevel parallelization on distributed memory machines are keys in order to find quantitative answers to nanoelectronics' most important questions. The previous incarnations of NEMO and OMEN have shown that such a task can be achieved.

NEMO5 aims to extend the previous efforts in the following directions.

1) Concurrent with the device downscaling, a diversification in the employed crystal growth directions and materials is observed. Although silicon and the traditional III–V alloys remain the workhorses of the industry, materials with wurtzite, trigonal, and other crystal structures gain importance as the attempts to achieve performance improvements become more creative. NEMO5 is designed to be completely versatile in these regards.

Manuscript received May 15, 2011; accepted June 28, 2011. Date of current version November 9, 2011. This work was supported in part by Grant EEC-0228390 of the National Science Foundation (NSF) that funds the Network for Computational Nanotechnology, by NSF PetaApps Grant 0749140, and by the Semiconductor Research Corporation and Intel Corporation. The review of this paper was arranged by Associate Editor M. P. Anantram

S. Steiger was with the Network for Computational Nanotechnology, Purdue University, West Lafayette IN 47907 USA. He is now with Google Switzerland, 8002 Zurich, Switzerland (e-mail: steiger@purdue.edu).

M. Povolotskyi, H.-H. Park, T. Kubis, and G. Klimeck are with the Network for Computational Nanotechnology, Purdue University, West Lafayette IN 47907 USA (e-mail: mpovolot@purdue.edu; park310@purdue.edu; tkubis@purdue.edu; gekco@purdue.edu).

Color versions of one or more of the figures in this paper are available online at http://ieeexplore.ieee.org.

Digital Object Identifier 10.1109/TNANO.2011.2166164

2) Multiscale simulation, i.e., the ability to solve coupled equations with varying accuracy and complexity on different spatial domains, is becoming increasingly important. Effects of long-range strain, the coupling of classical and quantum transport domains, and the coupling of electrons, phonons, and phonon transport are such examples.
3) The past decade has brought a wealth of professional and mature open-source software packages that handle certain aspects of device simulation. Employing these packages has manifold advantages ranging from a well-developed user base to the outsourcing of problems related to parallel numerics and I/O.
4) Being a research code employed by changing generations of students, documentation, clarity, and modularity of the code are essential. Only when all these criteria are fulfilled, can junior researchers act as builders of individual modules and the code endure multiple generations of developers.
5) Special use cases of previous codes were made available through the online simulation portal nanoHUB.org [12], [13]. NEMO5 aims to unify the engines underlying these tools to enable simplified user support and bug fixes as well as to increase numerical performance.
6) The code is placed under a license that enables contributions from the research community as well as commercial companies. It can, therefore, harvest the synergies that arise from such collaborations.

There have been other successful projects in nanoelectronics modeling. *Nextnano* [14] is a set of codes based on continuum models that is widely popular amongst experimental researchers. In addition to Schrödinger–Poisson simulations, it computes drift-diffusion-type transport equations, optoelectronic properties such as emission and absorption spectra, and magnetic field effects. *Tibercad* [15] incorporates both continuum and atomistic models and couples them in a multiscale way. Its features include semiclassical transport, heat transport, and optical characteristics. *NanoTCAD ViDES* [16] is geared toward carbon-based structures and thin nanowires. NEMO5 differentiates itself in that it is targeted more toward purely electronic (as opposed to optoelectronic) applications. It can both simulate small structures on a personal workstation and large structures on supercomputers by massive parallelization techniques using an atomic-resolution full-band picture, which is often required to obtain a meaningful description of the device.

This paper is organized as follows. Section II discusses the simulator design as well as critical computational aspects, in particular the employed external packages and the approach to multilevel parallelization. Section III describes the currently implemented physical models and a few typical application examples. Section IV discusses briefly the outreach effort made to the nanoelectronics community before concluding remarks are made in Section V.

II. Simulator Layout

This section provides an overview on the computational aspects of the simulator. NEMO5 is written entirely in C++ and embeds a variety of portable open-source packages. It has been ported to various platforms, amongst which a Cray XT5 (*jaguarpf.ccs.ornl.gov*), a Sun Constellation Linux cluster (*ranger.tacc.utexas.edu*), Red Hat Enterprise Linux clusters (e.g. *rossmann.rcac.purdue.edu*), Debian Linux (*nanoHUB.org*), a standard Kubuntu 10.10 workstation, and Microsoft Windows 32-bit.

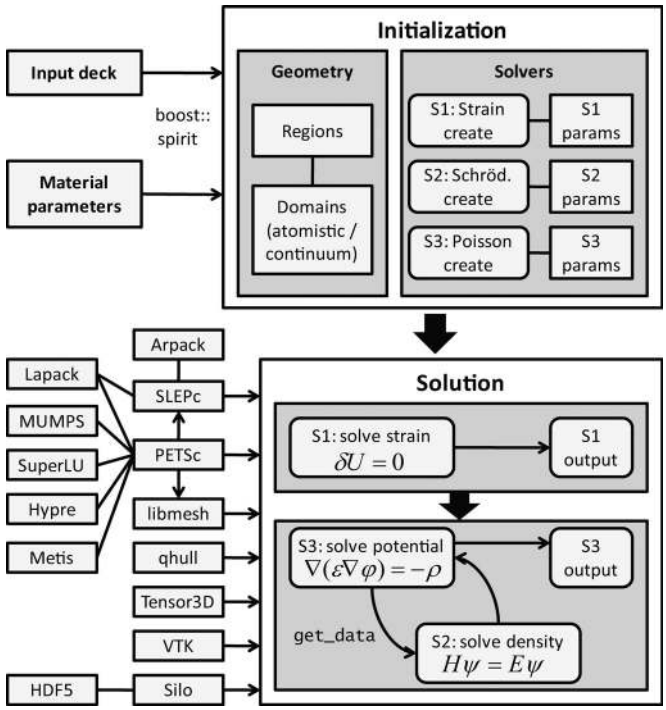

Fig. 1. NEMO5 simulation flow and employed packages.

A. Overall Simulation Flow

Fig. 1 sketches the simulation flow together with the employed external packages. We exemplify the flow for a self-consistent Schrödinger–Poisson simulation in a strained system. A simulation starts with the parsing of an input deck which provides information about the simulated structure as well as the desired type of simulation and the parameters for all required solvers. A *solver* is an individual module that performs a designated task, such as the solution of a specific physical equation. Three solvers are chosen for the example in Fig. 1: a strain solver (S1), a Schrödinger solver (S2), and an electrostatics solver (S3).

In a general initialization phase, geometrical *domains* are constructed on which equations are defined. A simulation can incorporate multiple conceptual domains and a mixture of continuum and atomistic representations. Every domain is partitioned into *regions* of different materials. A solver defines its equations on a solver-specific subset of a designated domain, its *active* regions. The task of the solver will be carried out only on activated regions. This enables multiscale simulations where compute-intensive equations are solved on subsets of the entire domain and simplified models are employed for the remaining regions.

Associated with every solver is a container where relevant material parameters are stored, and a designated section in the input deck where solver-specific parameters can be specified. Moreover, all solvers implement a simulator-wide interface for exchanging data with other solvers. This lets a solver become an autonomous module that performs a clear-cut task and is able to interact with other solvers. The modularity enables a user to mix and match physical modules and an easy switching between models by input deck instructions.

In the solution phase, some but not necessarily all solvers are executed sequentially. It may happen that the sole purpose of a solver is to provide input to another solver, while in other cases one solver may steer another. This happens for the case chosen in Fig. 1: the strain computation (S1) is done independently and prior to the self-consistent iteration between the density and the potential solvers. Here, we choose arbitrarily S3 (potential) to steer S2 (density) in that the potential solver does the self-consistent iteration as well as the solution of the Poisson equation. After every sequential solve phase, the results can be written to file.

B. Numerical Solvers

NEMO5 uses *PETSc* [17] for the solution of linear and nonlinear equation systems, and *SLEPc* [18] for eigenvalue problems (see Fig. 1). Both real- and complex-arithmetic versions are employed simultaneously. *PETSc* and *SLEPc* are mature and well-supported open-source projects that offer a plethora of MPI-parallel numerical algorithms. They also provide interfaces to other well-known packages like the parallel LU-factorization packages *MUMPS* [19] and *SuperLU* [20] as well as the sparse eigenvalue solver *PARPACK* [21]. *libmesh* [22] is employed for a finite-element solution of the Poisson equation and for higher order integration rules. *Qhull* [23] is used for the computation of Brillouin zones. Finally, *Tensor3D* [24] is used for small matrix-vector manipulations.

C. Input and Output

General steering of the simulator is done via a text file, the input deck, which is parsed using *boost::spirit.*[1] The material parameters are stored externally in a database, again based on *boost::spirit*, which is capable of parsing simple arithmetic expressions. This parsing functionality offers a convenient approach to analytical relationships and ternary or quaternary material parameter interpolation. An example for this is the Varshni formula [25] for the temperature dependence of the bandgap, which is written into the material parameter file in a transparent way. These small relationships can be conveniently and transparently adjusted by users. Material parameters can optionally be specified in the input deck to supersede the parameter file value. This enables parameter variations without having to edit or generate multiple parameter files.

Several output formats are available depending on the type of data. Atomistic data are saved in the *Silo*[2] or *VTK*[3] format. At this time, *VTK*'s XML-based parallel file formats are not interfaced; thus, *Silo* is the only choice for simulations with spatial parallelization. Atomistic datasets can be visualized using the freely available programs *VisIt*[4] or *Paraview.*[5] For selected tasks, other formats, such as *XYZ*[6], *PDB*[7], and *OpenDX*[8], are also available. *VTK* is employed for continuum data such as the shape of a Brillouin zone. *MATLAB*-compatible text files are typically chosen for 1-D datasets.

D. MPI Parallelization

The increased availability of multicore architectures and computing clusters pushes the need for efficient, large-scale parallel code. Many typical simulation tasks in nanoelectronics can be parallelized well as they consist of a conglomerate of decoupled problems (for example, the computation of a band structure requires the solution of independent eigenvalue problems for every wavevector). NEMO5 includes a general parallelization class that handles the setup of multilevel parallelization hierarchies and the distribution of problems onto the available processes. This class can be utilized in all simulation types. Together with spatial-domain decomposition techniques, this enables the solution of large problems using thousands of cores.

Fig. 2 shows an example of the distribution of eight available MPI processes in a three-level parallelization hierarchy. The three levels consist of the spatial-domain decomposition, a variable $V \in \{V_1, V_2\}$ and for each setting of V, a variable $k \in \{k_1, k_2\}$. In general, the computational load of each k-point may be known *a priori* to be unequal, as indicated by the values L in the figure.

As a first step, a real-space partitioning of the simulation domains is carried out (four partitions in Fig. 2). Spatial partitioning is usually determined in advance by the user and enables the treatment of much larger structures. Currently, 1-D and 3-D regular grid partitioning is supported. A user may 1) choose the exact positions of the partition boundaries or 2) just specify the total extension of the device and a desired total number of processes for the partitioning, leaving the partitioning to NEMO5. In this case, the partition boundaries are determined from a minimization of the interfaces between partitions.

In the example of Fig. 2, the two resulting replicas u_1 and u_2 can then be distributed onto the two remaining parallelization levels in a top-down fashion by choosing between the different strategies illustrated in Fig. 2(a) and (b). In the *scatter* strategy, one parallelization point after the other is assigned to the MPI process which has the least load, starting with the highest load points. The loads are *a priori* estimates that are set by the developer or default to one unit per bottom parallelization node. In the *cluster* strategy, which is available only for the intermediate level V, processes are grouped together rather than distributed. In the chosen example, this results in every point V_i retaining two processes, which can then be used for parallelization on

[1] http://www.boost.org
[2] https://wci.llnl.gov/codes/silo/
[3] http://www.vtk.org
[4] https://wci.llnl.gov/codes/visit/
[5] http://www.paraview.org
[6] http://openbabel.org/wiki/XYZ
[7] http://www.wwpdb.org/docs.html
[8] http://www.opendx.org

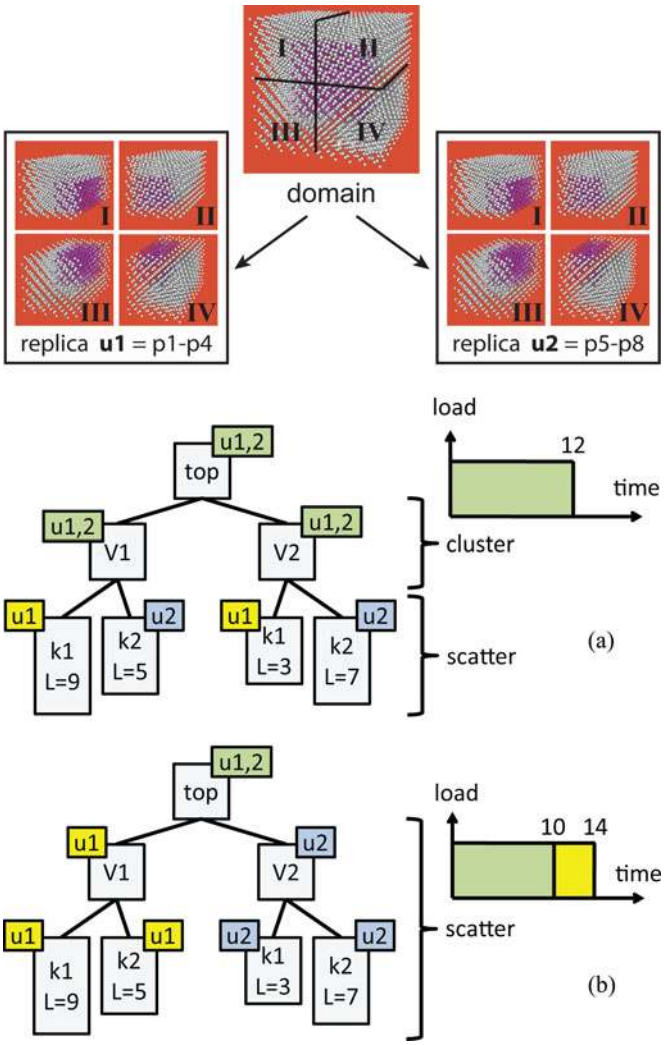

Fig. 2. Parallelization and MPI process distribution strategies in NEMO5. In the shown example 8, MPI processes are distributed onto a three-level parallelization scheme using a spatial-domain decomposition of four processes per replica. (a) Mixed cluster-scatter strategy outperforms (b) the pure scatter strategy in that the estimated computation time is less.

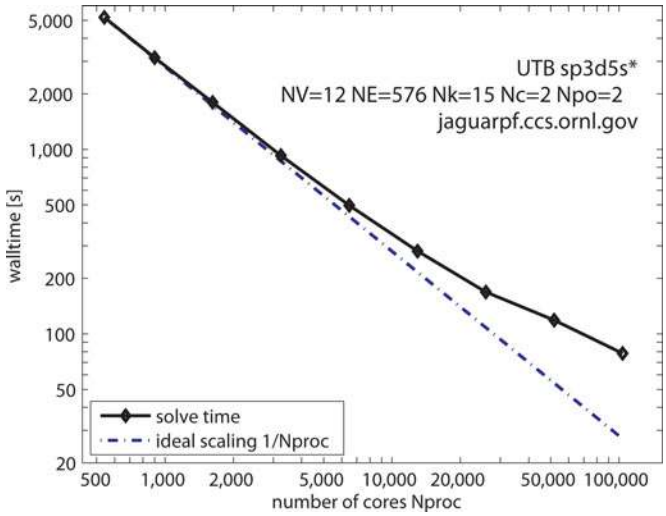

Fig. 3. Strong scaling behavior (solve time versus number of MPI processes N_{proc}) of a ballistic transport simulation in an ultrathin-body transistor. The simulation consists of $N_V = 12$ voltage points for which $N_E = 576$ energy points, $N_k = 15$ wavevector points, and self-energies at $N_c = 2$ contacts need to be solved, resulting in a maximum parallelization of $N_V N_E N_k N_c = 207,360$. The entire simulation needs 6e15 double-precision floating point operations. Displayed is the solve time for $N_{po} = 2$ Poisson iterations.

the level below. Conversely, any given process now needs to solve two V-points sequentially rather than a single one. In the shown example, this strategy is favorable as it provides a better overall load balancing and shorter estimated simulation time, as illustrated by the time-dependent load sketches.

The described approach constitutes a multilevel parallelization module that is decoupled from the physical meaning of the variable to be parallelized, provides good load balancing, and can be utilized in many different types of simulations. To demonstrate its utility, Fig. 3 shows the scaling of a quantum transport simulation which employs a four-level parallelization (voltages, energies, wavevectors, and contacts). In strong scaling experiments, the total numerical complexity is kept constant as the number of CPUs is increased. The result was obtained on the supercomputer *Jaguar* and shows good, but not yet perfect scaling behavior. Scaling with less than 1000 cores is near-perfect. Efforts are under way to optimize the scaling behavior at higher core numbers to the levels obtained by OMEN [8].

III. Physical Models

This section illustrates the physical models currently implemented in NEMO5. Each model subsection also discusses the validation process to ensure the implementation correctness.

The models presented here often exhibit different length scales and different computational complexities. For example, a calculation of an atomistically resolved strain profile can be achieved for structures of the size $(100\ \mathrm{nm})^3$ using current resources. The long-range strain will influence a central device domain, as has been shown with NEMO-3D [26]. On the contrary, an investigation of incoherent carrier–carrier scattering mechanisms on a micrometer length scale is neither feasible nor desirable, as most of the system is more adequately described by an incoherent and equilibrated carrier population. NEMO5 has the ability to couple together results obtained for domains of varying size. Fig. 4 illustrates this multiscale and multiphysics aspect. Electrostatics and effective-mass band structure models are continuum theories that have no concept of atoms as such, but they can be mixed with a density or discretization that is defined on an atomic lattice. Conversely, an atomistically resolved electrostatic potential, necessary for tight-binding calculations, can be obtained by interpolation from a coarser grid. A coupling of quantum transport with drift-diffusion has been demonstrated in NEMO-1D [27]. An example application for the multiscale and multiphysics capabilities of NEMO5 will be given in Section III-E.

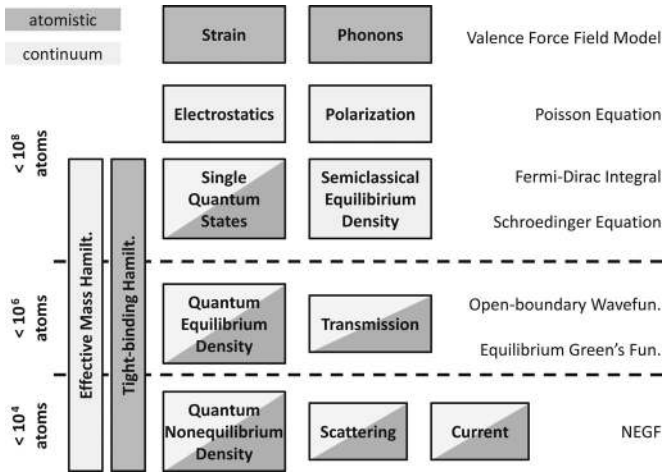

Fig. 4. Sketch of physical models included in NEMO5, illustrating the multi-scale aspect.

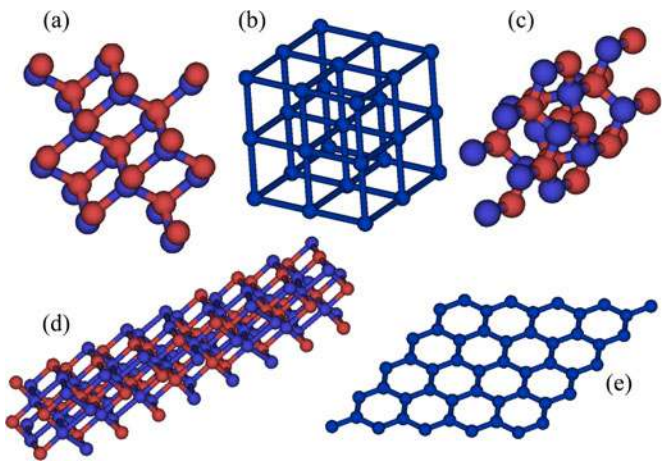

Fig. 5. Graphical depiction of different crystal structures: (a) zincblende, (b) simple-cubic, (c) wurtzite, (d) rhombohedral, and (e) graphene.

A. Crystal Structures

Atomistic simulations are at the core of the current capabilities of NEMO5. Fig. 5 displays the available crystallographic structures for such simulations. Diamond and zincblende structures (a) are the most common materials in nanoelectronics. The simple-cubic crystal structure (b) can be employed for effective-mass and other continuum theory simulations. Wurtzite-type materials (c), in particular nitrides, are employed in high-power applications as well as blue- and green-emitting optoelectronic devices. Rhombohedral (trigonal) unit cells (d) are important for thermoelectric devices. We have implemented the five-atomic basis that corresponds to bismuth telluride (Bi_2Te_3). The list is completed by carbon nanotubes and graphene (e).

The code is open for extensions to other crystal structures by specification of their primitive unit cell. It is currently limited to pseudomorphic arrangements, which can, however, contain cavities.

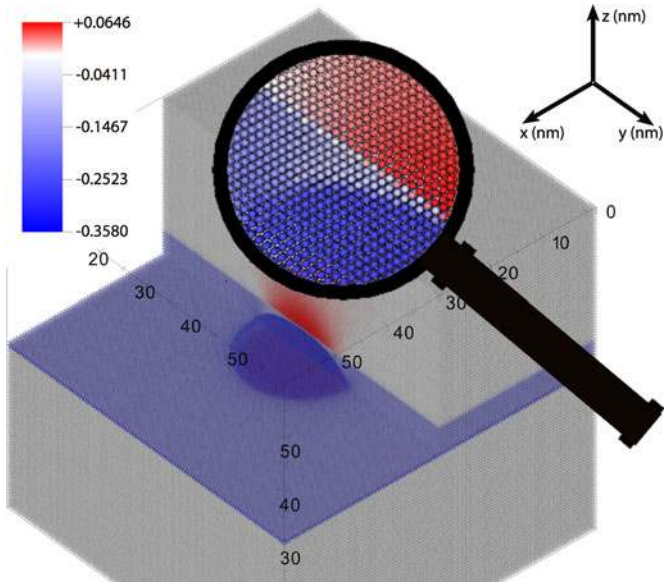

Fig. 6. Biaxial strain $\epsilon_{xx}+\epsilon_{yy}-2\epsilon_{zz}$ in a dome-shaped InAs quantum dot embedded in (60 nm)^3 of GaAs, computed with the Keating VFF model [28]. Visualization was done on the Dell XD Visualization cluster *longhorn.tacc.utexas.edu*.

B. Strain and Phonons

Nanostructures composed of materials with different lattice constants exhibit strain. NEMO5 is able to compute the strain-induced displacements of atoms using an extended version of the valence force field (VFF) model [29] in which the lattice energy is expressed in terms of atomic bond angles and lengths together with various microscopic spring constants. The energy functional implemented in NEMO5 features contributions from stretching, bending, cross-stretch, stretch-bend, and second-nearest-neighbor angle-angle interactions. These contributions can be turned on and off by the user in a mix and match fashion. For polar materials, the long-range Coulomb interaction can be added in the case of 0-D (bulk) and 3-D (confined) simulations.

Energy minimization is performed by a Newton iteration on the nonlinear equation system $\nabla U(\mathbf{d}_1,\ldots)=\mathbf{0}$, where U is the energy functional expressed in the atomic displacement coordinates $\mathbf{d}_i$. Contrary to continuum elasticity theory, the energy in the VFF model is only quasi-harmonic such that the solution process requires the solution of multiple linear equation systems. The Jacobian of the Newton iteration is computed analytically by taking the Hessian of the energy functional. This ensures quadratic convergence in the proximity of the solution. Even for large structures, the Newton iteration process typically takes five iterations or less. The strain tensor at any atomic site is obtained from the deformation of the tetrahedron constituted by its nearest neighbors (see [30, (19)]).

As a simulation example, Fig. 6 shows the biaxial strain $\epsilon_{xx}+\epsilon_{yy}-2\epsilon_{zz}$ occurring in a lens-shaped InAs quantum dot embedded in a large GaAs matrix [4]. The dot sits on top of a wetting layer and is surrounded by an InGaAs stress-reducing layer modeled in virtual crystal approximation. The dot has a

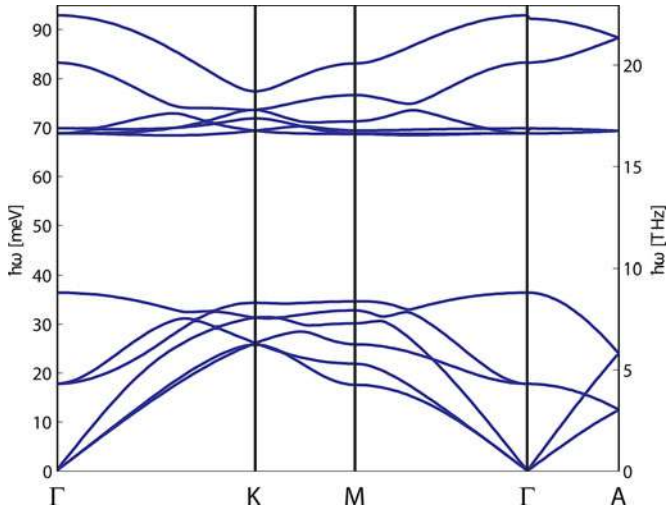

Fig. 7. Phonon dispersion of bulk α-GaN using the Keating VFF model augmented with the long-range Coulomb interaction.

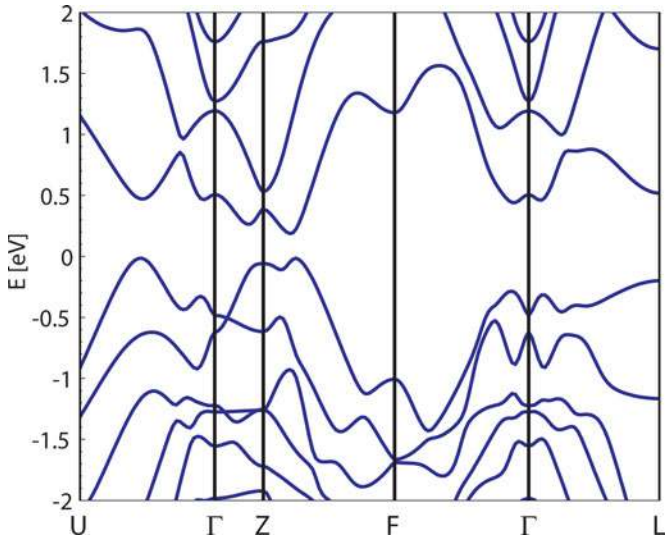

Fig. 8. Band structure of bulk Bi_2Te_3 calculated using the $sp^3s^*d^5$ tight-binding model and the parameters in [34].

20-nm diameter and a 5-nm height. The Keating energy functional using the parameters in [28] is used for these results. The system features a total of over 10 million atoms, and the linear equation system is distributed over 96 MPI processes. Due to the periodic boundary conditions on the sides and the free-floating top surface, the system is ill conditioned and even with preconditioning about 17 000 matrix-vector multiplications are required for the iterative solutions of the linear equation systems, bringing the solution time up to about 3.5 h. Solution with all-fixed surfaces takes only about 2 800 iterations or 25 min. In both cases, four Newton iterations are needed until convergence is reached.

The dynamical matrix of the lattice can be found from the Hessian of the energy functional by multiplication with appropriate phase factors. NEMO5 uses this dynamical matrix to compute phonon modes. Fig. 7 shows the bulk phonon dispersion of wurtzite-structure gallium nitride obtained from a Keating energy functional augmented by the long-range Coulomb interaction [31].

Validation process for strain and phonon calculations: Bulk phonon dispersions were validated for silicon [32], β-GaN [33], and α-GaN [31], with literature figures having no visible deviation from NEMO5 simulation results. Quadratic convergence in the proximity of the solution is observed in the Newton iteration of the strain relaxation, which validates the consistency between the computed gradient and the Hessian of the energy functional. The Hessian of the strain relaxation is computed by the same code that computes the dynamical matrix, thus providing an additional validation layer. Finally, biaxial strain computed in a quantum well was shown to agree with analytical results in the limit of small strain [30].

C. Electronic Structure

NEMO5 aims at the simulation of realistically extended nanoscale devices. The semiempirical tight-binding formalism using nearest-neighbor coupling offers an attractive compromise between computational cost and accuracy of the obtained results. It has been the workhorse of NEMO-1D, NEMO-3D, and OMEN and has been extensively validated. The atomistic representation of this method allows for an accurate treatment of material interfaces, alloy disorder and randomness, and structural roughness. Crystal symmetries are represented correctly and the obtained equations are much less numerically expensive compared to *ab initio* methods.

Fig. 8 displays the bulk band structure of Bi_2Te_3 computed using nearest-neighbor $sp^3s^*d^5$ orbitals and parameters from [34]. NEMO5 is able to compute electronic structures in pseudomorphically grown nanostructures using any of the aforementioned crystal systems (see Fig. 5). A compact and general expression of the tight-binding Hamiltonian in the two-center approximation [35] enables the rapid addition of tight-binding models that are not yet explicitly implemented.

An important aspect in tight-binding calculations of states in finite structures is the passivation of dangling bonds at physical surfaces. NEMO5 generalizes the general passivation scheme of [36] to apply to all crystal structures. The method is also able to treat nontrivial passivation atoms or molecules. This new method will be described in more detail elsewhere.

The simulator also implements a simple effective mass Hamiltonian. The obtained quantum states can further be used to calculate optical matrix elements and absorption spectra. A limited version of this functionality is made available through the educational tool *Quantum Dot Lab* on nanoHUB.org [37] (see Section IV). Fig. 9 shows a visualization of electron states in a spherical quantum dot obtained using this tool. nanoHUB provides online simulation capabilities through standard web browsers without the need of any additional installation steps.

Validation process for band structure calculations: A comparison of bulk tight-binding band structures against the literature [38]–[41] showed either no visible deviation against published band structure graphs or, when available, agreement up to numerical accuracy in figures of merit like band edges and

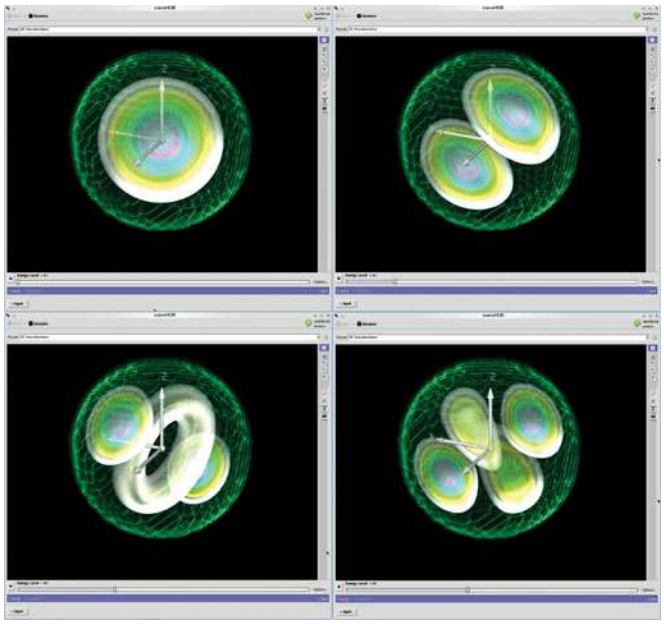

Fig. 9. Visualization of s-, p- and d-like electron states in a spherical quantum dot using *Quantum Dot Lab* [37]. This online tool currently uses the effective mass approximation.

masses. Validation of bulk and nanowire dispersions against previously developed code [2], [42] gave agreement up to numerical errors as small as 10^{-11} eV. Effective mass results in confined structures [37] were validated against textbook results.

D. Self-Consistent Schrödinger–Poisson Solver

The Poisson equation is solved using a standard finite-element formulation with parallelepipedal elements being based on the atomic unit cells. This equation can be coupled with a density computation using a nonlinear iteration scheme [43] in which a dependence of the density on the potential is predicted and included as part of a Newton iteration. This iteration scheme is often necessary to obtain convergence of the coupled potential-density equation system. One important aspect is that the density computation can be achieved using different physical models in a separate solver: for example, a semiclassical equilibrium density assuming locality and parabolic bands; a quantum equilibrium density obtained from a solution of the closed-boundary Schrödinger equation using a constant Fermilevel; a nonequilibrium density using NEGF or open-boundary wavefunctions (see Section III-E); or a mixture of these options (multiphysics simulation).

Fig. 10 shows the self-consistent result obtained for a cross section of an AlGaAs-GaAs HEMT in equilibrium using different models for the charge density. Switching between these models is done easily by few modifications of the input deck. Simulations of this type are made available through the *1-D Heterostructure Tool* on nanoHUB.org [44] (see Section IV).

Validation process for Schrödinger–Poisson calculations: Several numerical solutions of the Poisson equation with analytical density profiles were validated against analytical results. Effective mass solutions in doped bulk regions were shown to agree with the expected analytical relation between Fermi level, band edge, and free carrier density. The self-consistent solution displayed in Fig. 10 was validated with an independently developed code (an earlier version of [44]).

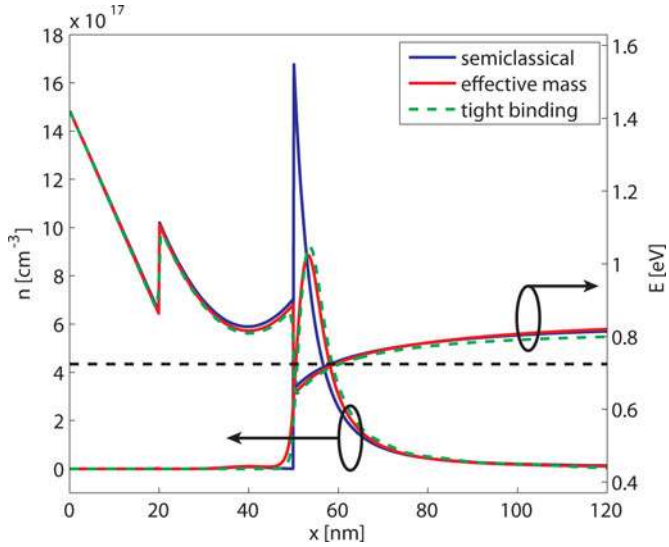

Fig. 10. Self-consistent Poisson-density solution of an HFET structure using different models for the density (*blue:* semiclassical, *red:* singleband effective mass, *green:* multiband $sp^3s^*d^5$ tight binding). The structure extends to 1 μm where it has a Dirichlet boundary condition for the potential. This structure is the default example of the *1-D Heterostructure Tool* on nanoHUB.org [44].

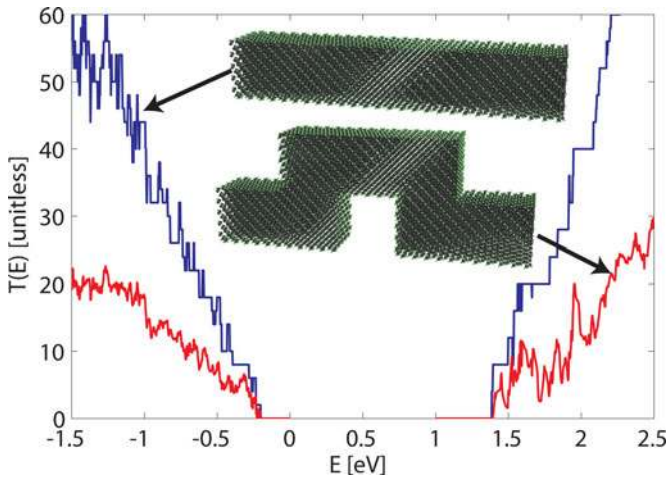

Fig. 11. Transmission through two Si nanowires with cross-section $(2.7\ \text{nm})^2$ using the 20-band $sp^3\ s^*\ d^5$ tight-binding model. The dangling bonds of the physical wire surface are passivated.

E. Transport

NEMO5 currently implements two approaches to quantum transport. The first approach [42] uses open-boundary wave functions and can be applied only in ballistic simulations. In the absence of scattering, this formalism is physically equivalent to Green's functions and outperforms NEGF simulations as only linear solves of a sparse matrix with multiple right-hand-side vectors are needed [42]. Fig. 11 shows the transmission through two Si nanowires with a cross section of $(2.7\ \text{nm})^2$ (5×5 cubic

unit cells) computed using the $sp^3s^*d^5$ tight-binding model with spin-orbit coupling. The bending of the second nanowire results in a reduction of the transmission and can be interpreted as a quantum resistance.

The second implemented approach to quantum transport uses NEGF [45], a many-body formalism capable of incorporating scattering and coherence loss. When being used in conjunction with a tight-binding Hamiltonian, the resulting computational cost is very large [46] and must be tackled with multilevel parallelization techniques. The recursive Green's function (RGF) algorithm, a numerical technique to compute necessary components of Green functions in two-terminal devices while avoiding explicit full matrix inversion, was generalized during the development of NEMO5 to multiple terminals and arbitrary geometric shapes and implemented in a highly parallelizable way. This opens up the investigation of structures with advanced geometries, such as the contact injecting regions in HEMTs, and multiterminal effects like MOSFET gate leakage. Details of this generalized RGF method will be published elsewhere.

Electron scattering plays an important role in the analysis of transport characteristics. Phase-conserving scattering mechanisms, such as interface roughness scattering or random alloy scattering, can be treated by direct modification of the tight-binding Hamiltonian. The single currently implemented phase-breaking scattering mechanism is electron–phonon scattering based on the deformation-potential description of [47]. This is the dominant mechanism in nonpolar materials such as Si.

It was shown in the past that sophisticated quantum transport models can be successfully coupled with simpler, less demanding continuum models to obtain reasonably accurate results in a much shorter amount of time [27], [48]. An example of such a multiscale, multiphysics simulation is shown in Fig. 12. At low and moderate voltages, the current flow through an RTD is governed by a single coherent quantum state bound to the central region. This state needs to be well resolved in energy and requires an energy discretization that adapts to the resonance. The regions outside the barriers are dominated by high carrier density, equilibration, and coherence loss. A full quantum simulation of this device would hence consist of an NEGF calculation that includes electron–electron and electron–phonon interactions in order to fill the triangular-shaped region in front of the first barrier. This notch has been shown to contribute significantly to the current [1], [48].

Instead of such an extremely expensive calculation, it is preferable to limit the region in which NEGF calculations are carried out to the well with its enclosing barriers and assume sufficient equilibration and coherence loss such that the injecting quantum states in the emitter and the collector (outside the RTD barriers) can be treated in local equilibrium and broadened by an empirical scattering rate [1], [48]. Hence, the exterior vicinity of the barriers can be treated with equilibrium Green's functions which account for the quantum density of states without the need of solving additional scattering self-energies. An additional approximation can be introduced by ignoring the quantum nature of the electrons altogether in the contact regions for the Poisson solution. The electrostatic potential can

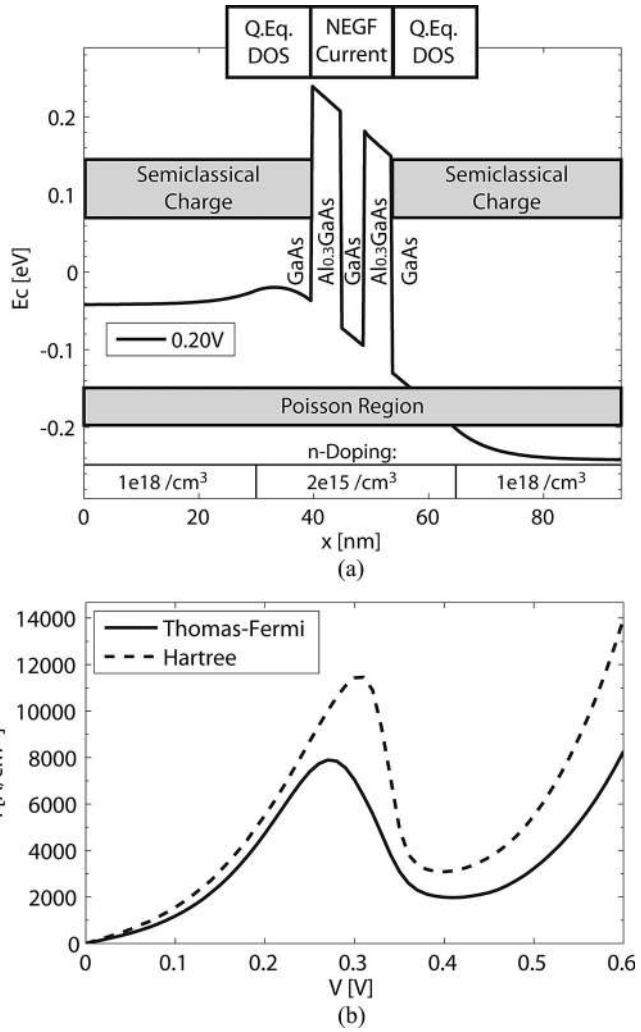

Fig. 12. Multiscale, multiphysics simulation of an RTD. (a) Sketch of the structure and involved physical regions and models for the electrostatic potential, charge, density of states (DOS) and current. The conduction band edge is shown at an applied voltage of 0.2 V. (b) Current–voltage characteristics. *Solid line:* Potential self-consistent with semiclassical density outside the barriers (termed *Thomas-Fermi* model). *Dashed line:* Potential self-consistent with semiclassical density outside the barriers and quantum density inside the barriers (termed *Hartree* model).

then be obtained from a fast self-consistent calculation with the semiclassical charge and serve as a fixed quantity for a one-step, non-self-consistent NEGF calculation of the current. The resulting simulation takes only seconds on a single CPU in the case of an effective mass basis and can already provide substantial insight into the mechanisms governing RTDs. Fig 12(b) shows the obtained current–voltage characteristics obtained with and without self-consistent inclusion of the quantum density in the potential, assuming an effective mass band model. These results can be duplicated in the tool *RTD Simulation with NEGF* on nanoHUB.org [49].

Finally, we show an example of a self-consistent calculation of ballistic quantum transport in an Si nanowire transistor (NWFET) in Fig. 13. Such devices are considered as potential candidates for the post-CMOS age due to excellent electrostatic control [11]. In the example, the cross section of the electronic

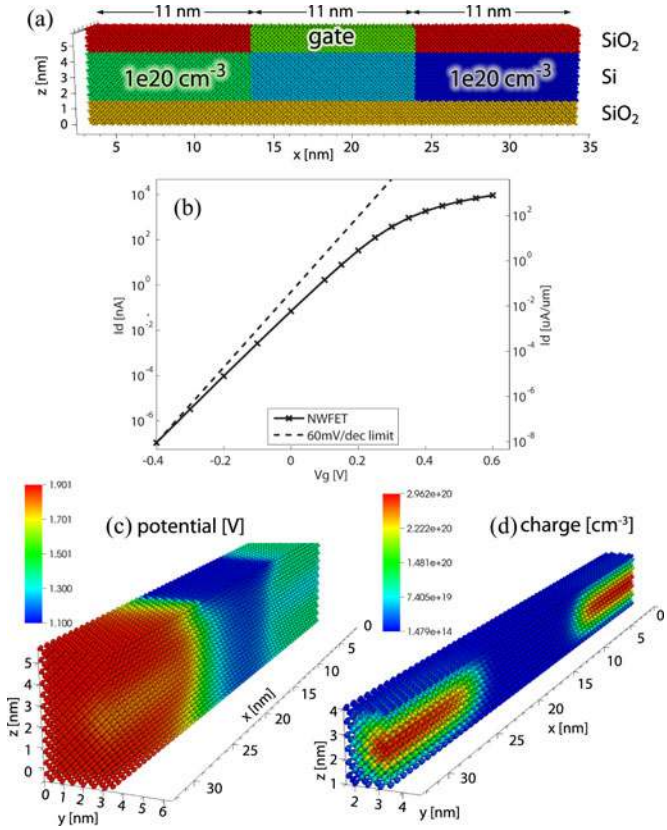

Fig. 13. Self-consistent calculation of transport through an Si nanowire transistor. (a) Electrostatic potential and (b) charge density obtained at $V_g = 0.2$ V. This ballistic result was obtained with the open-boundary wavefunction formalism using an $sp^3s^*d^5$ tight-binding band model excluding spin-orbit coupling. The electron density computation is restricted the silicon region.

domain is a square of the size $(3\ \text{nm})^2$, surrounded by oxide with an extension of $(6\ \text{nm})^2$. The length of the device is 30 nm. A trigate of 11-nm length is located at the three surfaces in the middle of the structure [see green-colored top area in Fig. 13(a)]. The high confinement and multivalley interactions of electrons necessitate an atomistic full-band description of the device. Here, the spinless $sp^3s^*d^5$ model is chosen for the device as it is dominated by the conduction band and not significantly influenced by the spin-orbit interaction. Even the five-band sp^3s^* model cannot capture the correct physics as it yields incorrect bands in the vicinity of the X-valleys (more specifically, the band structure is flat between the X and W points of the Brillouin zone [38]). Simulations of this type are computationally demanding and need to be carried out on parallel computers. The quantum transport calculation is carried out only in the silicon, with hard-wall boundary condition at the Si/SiO_2 interface. The gate voltage has been normalized to a condition of $I_{\text{off}}(V_g = 0V) = 0.1\frac{A}{m}$. A source–drain bias of 0.5 V is applied.

Validation process for transport calculations: Mode onsets in nanowire transmission spectra were compared to solutions of a periodic Schrödinger equation. The transmission over a step-like barrier was shown to agree with the analytical textbook formula for the effective mass case. The current–voltage characteristics of Fig. 12 coincide with results obtained by NEMO-1D [1] up to numerical errors which are not visible on the scale of the figure. A standard $n^+/n/n^+$ simulation example was shown to agree with the literature [45], with no visible deviation in the density, current–voltage, and potential graphs. Self-consistent current–voltage characteristics of an ultrathin-body transistor were shown to agree with OMEN, although small deviations remain that are likely to be due to differences in the simulated structure.

IV. Community Outreach and Availability

NEMO5 is placed under licenses that enable free distribution and collaboration with academics. Distribution of the source code is limited to close collaborators at this stage of development. Certain use cases are accessible without the need of any installation process through the portal nanoHUB.org [12]. At the time of writing, this includes an educational tool to calculate electronic states and absorption curves in quantum dots of different shapes using the effective mass approximation (*Quantum Dot Lab* [37]), a 1-D Schrödinger–Poisson solver (*1-D Heterostructure Tool* [44]), a tool to visualize Brillouin zones (*Brillouin Zone Viewer* [50]), and a tool to visualize unit cells and lattices (*Crystal Viewer Tool* [51]). Two more tools (*RTD Simulation with NEGF* [49] and *Band Structure Lab* [52]) are under development to have their engines replaced with NEMO5.

V. Conclusion

This paper presents NEMO5, a multipurpose simulation tool for nanoelectronics problems ranging from quick educational exercises to massively parallel simulations for state-of-the-art research. The selected simulation examples demonstrate the versatility of the code regarding the treatment of lattices with different crystal structures and different problem dimensionalities. The majority of implemented physical models currently uses an atomistic structure representation, although this is not a principal limitation of the code. Within the atomistic picture, current capabilities include large-scale simulations of strain, polarization, quantum states, self-consistent potential-density simulations, and quantum transport.

Future work will include continued refinement and optimization of existing functionality, focusing on user needs. It will also target the implementation of additional scattering mechanisms, more diverse nonpseudomorphic structures, and additional continuum models to extend multiscale simulation capabilities. Finally, novel techniques will be explored to reduce computational complexity.

During the development, emphasis was put on code documentation, validation, and modularity to facilitate transitions of developers and students. The exclusive reliance on portable open-source packages and the license enable academic institutions as well as industrial partners to use and extend the tool. The modularity enables a user to mix and match physical models and perform multiscale, multiphysics simulations. It also permits developers to extend or add modules while benefiting from access to existing input/output, numerical solver, parallelization, and geometry construction modules. It is the hope of the

developers that these synergetic effects give the code the potential to become a widely used tool throughout both the modeling community and experimental groups, pushing further the field of nanoelectronics.

ACKNOWLEDGMENT

The authors would like to thank Z. Jiang, B. Haley, D. Areshkin, L. Zeng, A. Goud, J. M. Sellier, X. Sun, and L. Bjaalie for their contributions to parts of the project. They also thank M. Luisier, S. Lee, A. Paul, H. Ryu, T. Boykin, C. Bowen, R. Veprek, and R. Kotlyar for stimulating discussions. Computational resources on nanoHUB.org as well as on *Jaguar* at the Oak Ridge National Laboratory (ORNL, INCITE project NEL001) are acknowledged. The authors furthermore acknowledge the Texas Advanced Computing Center (TACC)[9] at The University of Texas at Austin for providing visualization resources.

REFERENCES

[1] R. Lake, G. Klimeck, R. C. Bowen, and D. Jovanovic, "Single and multiband modeling of quantum electron transport through layered semiconductor devices," *J. Appl. Phys.*, vol. 81, pp. 7845–7869, 1997.

[2] G. Klimeck, S. Ahmed, H. Bae, N. Kharche, S. Clark, B. Haley, S. Lee, M. Naumov, H. Ryu, F. Saied, M. Prada, M. Korkusinski, T. B. Boykin, and R. Rahman, "Atomistic simulation of realistically sized nanodevices using NEMO 3-D—Part I: Models and benchmarks," *IEEE Trans. Electron. Devices*, vol. 54, no. 9, pp. 2079–2089, Sep. 2007.

[3] G. Klimeck, S. Ahmed, N. Kharche, M. Korkusinski, M. Usman, M. Prada, and T. Boykin, "Atomistic simulation of realistically sized nanodevices using NEMO 3-D—Part II: Applications," *IEEE Trans. Electron Devices*, vol. 54, no. 9, pp. 2090–2099, Sep. 2007.

[4] M. Usman, H. Ryu, I. Woo, D. Ebert, and G. Klimeck, "Moving toward nano-TCAD through multimillion-atom quantum-dot simulations matching experimental data," *IEEE Trans. Nanotechnol.*, vol. 8, no. 3, pp. 330–344, May 2009.

[5] G. Lansbergen, R. Rahman, C. Wellard, I. Woo, J. Caro, N. Collaert, S. Biesemans, G. Klimeck, L. Hollenberg, and S. Rogge, "Gate-induced quantum-confinement transition of a single dopant atom in a silicon FinFET," *Nature Phys.*, vol. 4, no. 8, pp. 656–661, 2008.

[6] S. Lee, H. Ryu, Z. Jiang, and G. Klimeck, "Million atom electronic structure and device calculations on peta-scale computers," presented at the 13th Int. Workshop Comput. Electron., Beijing, China, 2009.

[7] G. Klimeck and M. Luisier, "Atomistic modeling of realistically extended semiconductor devices with NEMO and OMEN," *Comput. Sci. Eng.*, vol. 12, no. 2, pp. 28–35, 2010.

[8] M. Luisier and G. Klimeck, "Numerical strategies towards peta-scale simulations of nanoelectronics devices," *Parallel Comput.*, vol. 36, no. 2–3, pp. 117–128, 2010.

[9] M. Luisier and G. Klimeck, "Simulation of nanowire tunneling transistors: From the Wentzel–Kramers–Brillouin approximation to full-band phonon-assisted tunneling," *J. Appl. Phys.*, vol. 107, no. 8, pp. 084 507–084 507, 2010.

[10] N. Kharche, G. Klimeck, D. Kim, J. A. del Alamo, and M. Luisier, "Multiscale metrology and optimization of ultra-scaled InAs quantum well FETs," *IEEE Trans. Electron Devices*, vol. 58, no. 7, pp. 1963–1971, Jul. 2011.

[11] M. Luisier and G. Klimeck, "Atomistic full-band simulations of silicon nanowire transistors: Effects of electron-phonon scattering," *Phys. Rev. B*, vol. 80, no. 15, p. 155430, 2009.

[12] G. Klimeck, M. McLennan, S. Brophy, G. Adams III, and M. Lundstrom. (2008). "nanoHUB.org: Advancing education and research in nanotechnology," *Comput. Sci. Eng.*, pp. 17–23, [Online]. Available: http://www.nanoHUB.org

[13] A. Strachan, G. Klimeck, and M. Lundstrom, "Cyber-enabled simulations in nanoscale science and engineering," *Comput. Sci. Eng.*, vol. 12, PP. 12–17, 2010.

[14] S. Birner, T. Zibold, T. Andlauer, T. Kubis, M. Sabathil, A. Trellakis, and P. Vogl, "nextnano: General purpose 3-D simulations," *IEEE Trans. Electron Devices*, vol. 54, no. 9, pp. 2137–2142, Sep. 2007.

[15] M. Auf der Maur, M. Povolotskyi, F. Sacconi, A. Pecchia, G. Romano, G. Penazzi, and A. Di Carlo, "Tibercad: Towards multiscale simulation of optoelectronic devices," in *Numerical Simulation of Optoelectronic Devices (NUSOD)*, vol. 8, Nottingham, U.K.: IEEE Press, 2008, pp. 43–44.

[16] "Nanotcad vides," Oct. 2008. [Online]. Available: http://nanohub.org/resources/5116

[17] S. Balay, K. Buschelman, V. Eijkhout, W. Gropp, D. Kaushik, M. Knepley, L. McInnes, B. Smith, and H. Zhang, "PETSc users manual," Argonne Natl. Lab., Argonne, IL, 2003.

[18] V. Hernandez, J. E. Roman, and V. Vidal, "SLEPc: A scalable and flexible toolkit for the solution of eigenvalue problems," *ACM Trans. Math. Softw.*, vol. 31, no. 3, pp. 351–362, Sep. 2005.

[19] P. R. Amestoy, I. S. Duff, J.-Y. L'Excellent, and J. Koster. (2001). A fully asynchronous multifrontal solver using distributed dynamic scheduling. *SIAM J. Matrix Anal. Appl.* [Online]. *23(1)*, p. 15. Available: http://graal.ens-lyon.fr/MUMPS/

[20] J. W. Demmel, J. R. Gilbert, and X. S. Li. (1999). An asynchronous parallel supernodal algorithm for sparse gaussian elimination. *SIAM J. Matrix Anal. Appl.* [Online]. *20(4)*, p. 915. Available: http://crd.lbl.gov/xiaoye/SuperLU/

[21] K. Maschhoff and D. Sorensen. (1996). P_ARPACK: An efficient portable large scale eigenvalue package for distributed memory parallel architectures. *Appl. Parallel Comput. Ind. Comput. Optim.*, [Online]. pp. 478–486, Available: http://www.caam.rice.edu/software/ARPACK/

[22] B. S. Kirk, J. W. Peterson, R. H. Stogner, and G. F. Carey, "libMesh: A C++ library for parallel adaptive mesh refinement/coarsening simulations," *Eng. Comput.*, vol. 22, no. 3–4, pp. 237–254, 2006.

[23] C. Barber, D. Dobkin, and H. Huhdanpaa. (1996). The quickhull algorithm for convex hulls. *ACM Trans. Math. Softw. (TOMS)* [Online]. *22(4)*, pp. 469–483. Available: http://www.qhull.org

[24] T. van den Boogaard, "Tensor classes," (May 2011). [Online]. Available: http://www2.tm.ctw.utwente.nl/ ton/tensor.html

[25] I. Vurgaftman, J. R. Meyer, and L. R. Ram-Mohan, "Band parameters for iii-v compound semiconductors and their alloys," *J. Appl. Phys.*, vol. 89, pp. 5815–5875, 2001.

[26] M. Korkusinski and G. Klimeck, "Atomistic simulations of long-range strain and spatial asymmetry molecular states of seven quantum dots," *J. Phys.: Conf. Series*, vol. 38, pp. 75–78, 2006.

[27] G. Klimeck, "Quantum and semi-classical transport in nemo 1-D," *J. Comput. Electron.*, vol. 2, pp. 177–182, 2003.

[28] R. Martin, "Elastic properties of ZnS structure semiconductors," *Phys. Rev. B*, vol. 1, no. 10, pp. 4005–4011, 1970.

[29] M. Musgrave and J. Pople, "A general valence force field for diamond," *Proc. R. Soc. Lond. Series A, Math. Phys. Sci.*, vol. 268, no. 1335, pp. 474–484, 1962.

[30] C. Pryor, J. Kim, L. Wang, A. Williamson, and A. Zunger, "Comparison of two methods for describing the strain profiles in quantum dots," *J. Appl. Phys.*, vol. 83, pp. 2548–2554, 1998.

[31] S. Yamakawa, R. Akis, N. Faralli, M. Saraniti, and S. Goodnick, "Rigid ion model of high field transport in GaN," *J. Phys.: Cond. Matter*, vol. 21, p. 174206, 2009.

[32] A. Paul, M. Luisier, and G. Klimeck, "Modified valence force field approach for phonon dispersion: From zinc-blende bulk to nanowires," *J. Comput. Electron.*, vol. 9, pp. 160–172, 2010.

[33] J. Zi, X. Wan, G. Wei, K. Zhang, and X. Xie, "Lattice dynamics of zinc-blende GaN and AlN: I. Bulk phonons," *J. Phys.: Cond. Matter*, vol. 8, p. 6323, 1996.

[34] S. Lee and P. von Allmen, "Tight-binding modeling of thermoelectric properties of bismuth telluride," *Appl. Phys. Lett.*, vol. 88, p. 022107, 2006.

[35] A. V. Podolskiy and P. Vogl, "Compact expression for the angular dependence of tight-binding hamiltonian matrix elements," *Phys. Rev. B*, vol. 69, no. 23, p. 233101, Jun. 2004.

[36] S. Lee, F. Oyafuso, P. von Allmen, and G. Klimeck, "Boundary conditions for the electronic structure of finite-extent embedded semiconductor nanostructures," *Phys. Rev. B*, vol. 69, no. 4, p. 045316, Jan. 2004.

[37] (2005, Nov.). Quantum dot lab, doi:10254/nanohub-r450.10. [Online]. Available: http://nanohub.org/resources/450

[38] G. Klimeck, R. Chris Bowen, T. Boykin, and T. Cwik, "sp3s* Tight-binding parameters for transport simulations in compound semiconductors," *Superlattices Microstruct.*, vol. 27, no. 5–6, pp. 519–524, 2000.

[9] http://www.tacc.utexas.edu

[39] J. Jancu, R. Scholz, F. Beltram, and F. Bassani, "Empirical spds* tight-binding calculation for cubic semiconductors: General method and material parameters," *Phys. Rev. B*, vol. 57, no. 11, pp. 6493–6507, 1998.
[40] J. Jancu, F. Bassani, F. D. Sala, and R. Scholz, "Transferable tight-binding parametrization for the group-III nitrides," *Appl. Phys. Lett.*, vol. 81, pp. 4838–4840, Dec. 2002.
[41] T. Boykin, G. Klimeck, and F. Oyafuso, "Valence band effective-mass expressions in the sp3d5s* empirical tight-binding model applied to a Si and Ge parametrization," *Phys. Rev. B*, vol. 69, no. 11, p. 115201, 2004.
[42] M. Luisier, A. Schenk, W. Fichtner, and G. Klimeck, "Atomistic simulation of nanowires in the sp3d5s* tight-binding formalism: From boundary conditions to strain calculations," *Phys. Rev. B*, vol. 74, p. 205323, 2006.
[43] A. Trellakis, A. T. Galick, A. Pacelli, and U. Ravaioli, "Iteration scheme for the solution of the two-dimensional schroedinger-poisson equations in quantum structures," *J. Appl. Phys.*, vol. 81, pp. 7880–7884, 1997.
[44] (2008, Sep.). 1d heterostructure tool. doi:10254/nanohub-r5203.15. [Online]. Available: http://nanohub.org/resources/5203
[45] S. Datta, "Nanoscale device modeling: The green's function method," *Superlattices Microstruct.*, vol. 28, no. 4, pp. 253–278, 2000.
[46] M. Luisier, "A parallel implementation of electron-phonon scattering in nanoelectronic devices up to 95k cores," in *Proceedings of the 2010 ACM/IEEE International Conference for High Performance Computing, Networking, Storage and Analysis* (ser. SC'10). Washington, DC: IEEE Comput. Soc., 2010, pp. 1–11.
[47] S. Jin, Y. J. Park, and H. S. Min, "A three-dimensional simulation of quantum transport in silicon nanowire transistor in the presence of electron-phonon interactions," *J. Appl. Phys.*, vol. 99, p. 123719, 2006.
[48] G. Klimeck, R. Lake, R. Bowen, W. Frensley, and T. Moise, "Quantum device simulation with a generalized tunneling formula," *Appl. Phys. Lett.*, vol. 67, no. 17, pp. 2539–2541, 1995.
[49] "Resonant tunneling diode simulation with NEGF," (Sep. 2008) doi:10254/nanohub-r5237.28. [Online]. Available: http://nanohub.org/resources/5237
[50] (2011, Apr.). "Brillouin zone viewer," doi:10254/nanohub-r10545.1. [Online]. Available: http://nanohub.org/resources/10545
[51] (2008, Jan.). "Crystal viewer tool," doi:10254/nanohub-r3741.12. [Online]. Available: http://nanohub.org/resources/3741
[52] (2006, May). "Band structure lab," doi:10254/nanohub-r1308.17. [Online]. Available: http://nanohub.org/resources/1308

Sebastian Steiger was born in Kilchberg, Zurich, Switzerland, in 1981. He received the Diploma degree in physics and the Ph.D. degree in electrical engineering from the Swiss Federal Institute of Technology, Zurich, Switzerland, in 2005 and 2009, respectively.

His research interests include the implementation and application of models for nanoscale semiconductor devices. In 2010 and 2011, he was a Postdoctoral Researcher at the Network for Computational Nanotechnology, Purdue University, West Lafayette, IN. He is currently with Google Switzerland, Zurich.

Michael Povolotskyi received the M.Sc. degree in applied mathematics and physics from Moscow Institute of Physics and Technology, Moscow, Russia, in 2000, and the Ph.D. degree in electric engineering from the University of Rome "Tor Vergata," Rome, Italy, in 2004.

He continued his professional development as a Postdoctoral Researcher in "Tor Vergata" and in the Georgia Institute of Technology, Savannah. Since 2009, he has been with Purdue University, West Lafayette, IN, as a Research Assistant Professor in the electric engineering school. His research interests include the modeling of semiconductor nanostructures, devices, and high-power computing. He is a coauthor of electronic modeling software nextnano3, TiberCAD, and NEMO5.

Hong-Hyun Park received the B.S. and Ph.D. degrees in electrical engineering from Seoul National University, Seoul, Korea, in 2003 and 2009, respectively.

He was at the Nano-Systems Institute, Seoul National University, as a Researcher. He is currently a Postdoctoral Associate at Purdue University, West Lafayette, IN. His research interests include the modeling of electronic devices, semiclassical and quantum transport, and fluctuation and noise phenomena.

Tillmann Kubis was born in Ingolstadt, Germany, in 1978. He received the Diploma degree and the Ph.D. degree in physics from the Technical University of Munich, Garching, Germany, in 2004 and 2009, respectively.

He is currently a Postdoctoral Researcher at the Network for Computational Nanotechnology, Birck Nanotechnology Center, School of Electrical and Computer Engineering, Purdue University, West Lafayette, IN. His research interests include the modeling of realistic charge, spin and heat transport in semiconductor nanodevices, and optoelectronics using numerical implementations of the nonequilibrium Green's function formalism on atomic length scales.

Gerhard Klimeck (S'91–M'95–SM'04) received the Ph.D. degree from Purdue University, West Lafayette, IN, in 1994, and the German Electrical Engineering degree from Ruhr-University Bochum, Bochum, Germany, in 1990.

He is currently the Director of the Network for Computational Nanotechnology and Professor of electrical and computer engineering at Purdue University. He leads the development and deployment of web-based simulation tools, research seminars, tutorials, and classes that are hosted on http://nanohub.org a community website that is utilized by over 170 000 users annually. He coauthored 34 tools on nanoHUB that have been used by over 20 000 users. He was the Technical Group Supervisor for the Applied Cluster Computing Technologies Group and continues to hold his appointment as a Principal Member at the NASA Jet Propulsion Laboratory on a faculty part-time basis. Previously, he was a member of Technical Staff at the Central Research Lab of Texas Instruments. He has been the lead on the development of NEMO 3-D, a tool that enables the simulation of tens-of-million atom quantum-dot systems, and NEMO 1-D, the first nanoelectronic CAD tool. His work is documented in over 300 peer-reviewed publications and over 450 conference presentations. His research interest include the modeling of nanoelectronic devices, parallel cluster computing, and genetic algorithms.

Dr. Klimeck is a Fellow of the Institute of Physics and a member of American Physical Society, Eta Kappa Nu, and Tau Beta Pi.